BIOCHEMISTRY
including biophysical chemistry & molecular biology

Article

pubs.acs.org/biochemistry

A C-RING-like Domain Participates in Protein Self-Assembly and Mineral Nucleation

Fairland F. Amos, Moise Ndao, Christopher B. Ponce, and John Spencer Evans*

Laboratory for Chemical Physics, New York University, 345 East 24th Street, New York, New York 10010, United States

Supporting Information

ABSTRACT: AP7 is a nacre-associated protein of the mollusk shell that forms supramolecular assemblies that nucleate single-crystal aragonite in vitro. AP7 possesses two major sequence regions: a random coil 30-amino acid N-terminal domain (AP7N) and a partially disordered 36-amino acid C-terminal domain (AP7C) that exhibits imperfect sequence homology to the C subclass of the intracellular RING domain family. We report here new findings that implicate the C-RING domain in AP7-mediated supramolecular assembly and single-crystal mineral formation. AP7 protein spontaneously self-assembles over a pH range of 4−9 and is monomeric at pH >9.5. AP7N and AP7C both oligomerize over the pH range of 4−9, with the AP7C sequence closely resembling AP7 in terms of particle morphology and size. In vitro mineralization experiments demonstrate that both AP7N and AP7C form supramolecular assemblies that nucleate single-crystal calcium carbonates. Comparison of previously published nuclear magnetic resonance-based structures of AP7C and AP7N reveals the significant presence of complementary anionic−cationic electrostatic molecular surfaces on AP7C that are not found on AP7N, and this may explain the noted discrepancies between the two domains in terms of self-assembly and single-crystal nucleation. We conclude that the C-RING-like sequence is an important site for AP7 self-association and mineral nucleation, and this represents the first known instance of a RING-like sequence performing these functions within an extracellular protein.

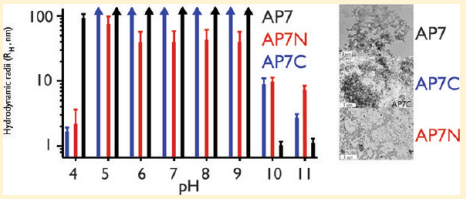

The formation of biominerals in Nature often requires the participation of specialized proteins that direct matrix assembly, nucleation, and crystal growth.[1−11] In many cases, the sequences of these specialized proteins are highly unique and often feature regions that do not correspond to the sequences of other known globular proteins.[1−11] However, imperfect sequence homologies exist between certain regions of biomineralization proteins and other non-mineral-associated proteins.[1,3−5] We will refer to these imperfect homologous domains as "imitator" domains, because they copy certain aspects of the globular sequence with less than perfect fidelity. Some recent examples have been identified in mollusk shell mineralization protein sequences, where regions partially homologous to acetylcholine-binding domains,[3] glycine loops,[1] and disulfide core domains[1] exist. For a number of reasons, little if any information regarding the true function of these imitator domains within biomineralization proteins is available. However, there is speculation that these domains perform functions that are not directly related to nucleation or crystal interaction.[3,5]

One interesting example of an imitator domain-containing biomineralization protein is AP7 (7.5 kDa, *Haliotis rufescens*).[5,11,15−17] This intrinsically disordered[12−14] nacre layer protein forms supramolecular complexes that nucleate single-crystal and lamellar aragonite.[11] The phenomenon of protein supramolecular complexes stabilizing aragonite has also been noted for other nacre protein sequences.[18−20] The AP7 sequence consists of a random coil 30-amino acid N-terminal region (1−30, AP7N)[5,11,15−17] and a partially structured 36-amino acid C-terminal region (31−66, AP7C) (Figure 1). It is this C-terminal domain that is most interesting, for it exhibits partial homology (<50%)[15] to an interesting subset of carboxy-terminal Cys-rich Zn binding motifs known as the C-RING (really interesting new gene domain, C subclass)[21−24] and thus represents a putative imitator domain. Reported variants of the RING domain family occur in more than 400 proteins, and many of these domains are typically involved in mediating protein−protein interactions within eukaryotic cells.[21−24] Thus, the occurrence of a C-RING-like sequence within an extracellular biomineralization protein is highly intriguing, and it has been suggested that this sequence participates in the formation of mineralized AP7 supramolecular assemblies.[11] However, this hypothesis has not yet been confirmed.

In this paper,we report new experiments that establish the functional relevance of the C-RING-like imitator sequence within AP7. Like other nacre protein sequences,[18−20] we confirm that AP7, AP7N, and AP7C all oligomerize in solution in the pH range of 4.0−9.5. However, it is the C-RING-like AP7C that most closely resembles the AP7 protein in terms of supramolecular assembly morphology and oligomer particle size. In vitro mineralization studies confirm that both AP7N and AP7C assemblies nucleate single-crystal calcium carbonates in vitro. Solvent accessible surface analysis of published nuclear magnetic resonance (NMR)-determined AP7N and AP7C structures[15,17] reveals that AP7C possesses complementary

Received: June 2, 2011
Revised: September 16, 2011
Published: September 19, 2011

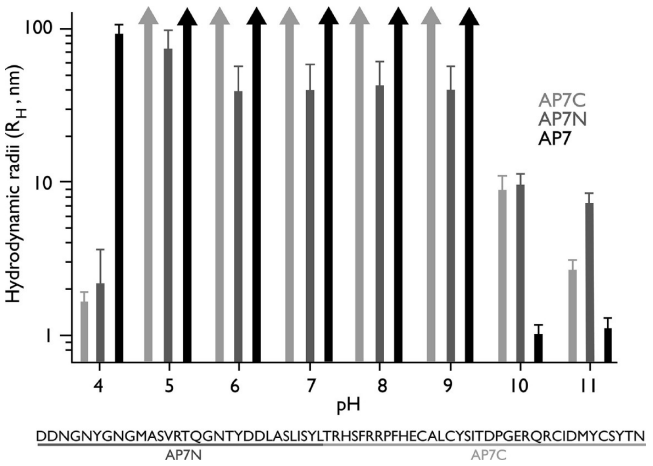

Figure 1. Histogram comparison of particle size distributions obtained for apo-AP7, AP7C, and AP7N polypeptides in aqueous buffers over the pH range of 4−11. The error bars represent the skewed polydispersity of the particles. The arrows indicate that the R_H values for a particular pH value are out of range for the DLS instrument. Results obtained in the presence of 12.5 mM $CaCl_2$ are identical to that presented here for the apo states. The primary amino acid sequence of AP7 is shown below the graph, along with the AP7N (1−30) and C-RING AP7C (31−66) sequence regions.

anionic−cationic molecular surfaces that are not found within AP7N, and this may explain the significant pH-dependent oligomerization of both AP7C and AP7. We conclude that the AP7 C-RING-like sequence contributes to the self-assembly and nucleation activities of AP7, and this represents the first known instance of a C-RING-like sequence performing these functions within an extracellular protein.

MATERIALS AND METHODS

Synthesis and Purification of AP7, AP7N, and AP7C. The AP7 protein (Figure 1) was chemically synthesized using tBoc chemistry and purified as described previously.[11,16] Similarly, the protein fragments, AP7N (amino acids 1−30, free N-terminus, C-α amide capped) and AP7C (amino acids 31−66, *N*-acetyl-modified N-terminus, free C-terminus) (Figure 1), were synthesized using FMOC chemistries and purified as previously described.[5,15,17] The purified, thiol-containing AP7 and AP7C polypeptides were subsequently dissolved in H_2- and N_2-flushed unbuffered deionized distilled water (UDDW).[11,15,16] Aliquots were then stored at −20 °C in airtight sealed vials that were preflushed with highly pure N_2 gas. The AP7N peptide was stored in the lyophilized form at −20 °C until needed and was dissolved in UDDW immediately prior to the start of the experiments.[5,11,17]

Nacre Polypeptide Assembly and Calcium Carbonate Nucleation. Using supernatant sampling,[11,20] we recovered AP7N, AP7C, and AP7 mineralization clusters from mineralization assay solutions for TEM visualization and electron diffraction. These mineralization assays utilized 12.5 mM $CaCl_2$ (>98% pure, Sigma/Aldrich) in UDDW, with solid ammonium carbonate vapor (99% pure, Sigma/Aldrich) diffusion at 16 °C for 18 h.[8,11,15,18−20] Final peptide concentrations in these assays were 50 and 100 μM, corresponding to the protein concentrations that give rise to stabilized aragonite−protein complexes.[11,18−20] Two control conditions were utilized: no added peptide (negative control) and 5.4 μM (355 μg/mL) bovine serum albumin (BSA, >96% pure, 66 kDa, Sigma-Aldrich), a concentration that is consistent with that employed in previous mineralization studies.[19,20] For TEM studies, an aliquot (~10 μL) of the assay supernatant was removed at the end of the 16 h period and carefully spotted on a copper TEM grid [coated with a Formvar layer that is stabilized by carbon (Ted Pella, Inc.)].[11,20] This spot was gently washed with ethanol and UDDW, and then the grids were allowed to air-dry. TEM imaging and electron diffraction measurements were performed on grids using a Philips CM12 transmission electron microscope at 120 kV. Cropping of TEM images and adjustment of brightness/darkness and contrast levels were performed using Adobe Photoshop. For electron diffraction measurements, we obtained diffraction patterns for 10 crystals in each sample.

Dynamic Light Scattering. The hydrodynamic radii of AP7, AP7N, and AP7C were measured over a pH range of 4−11 using a DynaPro MS/X dynamic light scattering instrument (Protein Solutions, Inc.) and experimental protocols developed for nacre polypeptides.[18] The polypeptide samples were mixed in various 10 mM buffers (pH 4.0−6.0, sodium acetate/acetic acid buffer; pH 7.0−8.5, Tris-HCl buffer; pH 9.0−11.3, sodium carbonate/bicarbonate buffer), with final polypeptide concentrations of 100 μM. All samples were filtered using a 0.22 μm polyvinylidene fluoride syringe filter (Fisher) and then incubated at 16 °C for 10 min in the cuvette prior to measurement. Ten acquisitions were taken per pH point per sample. Data regularization analysis was performed using Dynamics version 6.0. By measuring the fluctuations in the laser light intensity scattered by the sample, the instrument is able to detect the speed (diffusion coefficient) at which the particles are moving through the medium. This value is converted to hydrodynamic radius (R_H) using the Stokes−Einstein relation:[25]

$$D = \frac{kT}{6\pi\eta R_H}$$

where D is the diffusion coefficient, k is Boltzmann's constant, T is the absolute temperature, η is the viscosity, and R_H is the sphere-equivalent hydrodynamic radius.[25]

NMR Studies of Monomeric and Oligomeric AP7. To compare the degree of intermolecular association within AP7 oligomers, we performed solution NMR experiments on 100 μM samples [90% (v/v) UDDW and 10% (v/v) D_2O (99.9% pure) (Cambridge Isotope Laboratories, Inc.)] at pH 4.0 and 10.0, corresponding to the predominantly assembled and monomeric states, respectively, as determined by our DLS experiments. Two-dimensional proton NMR spectroscopy (TOCSY and NOESY) was conducted at 298 K on a 900 MHz ultrashield Bruker US^2 AVANCE spectrometer (21.14 T superconducting magnet) outfitted with a 5 mm HXY triple-resonance Bruker cryoprobe. The ^{1}H 90° pulses were 8.04 and 8.90 μs for AP7 at pH 4 and 10, respectively; the relaxation delay was 1.5 s, and a spectral width of 12 ppm was used. Water suppression was achieved using gradient excitation sculpting. TOCSY experiments were performed with mixing times of 60, 70, 75, and 80 ms, while NOESY experiments were performed with mixing times of 50, 100, 150, and 200 ms. The data were collected for 2048 complex points and transformed and visualized using NMRPipe (National Institutes of Health, Bethesda, MD) and Sparky (Sparky 3, University of California, San Francisco, CA).

dx.doi.org/10.1021/bi201346d | *Biochemistry* 2011, 50, 8880−8887

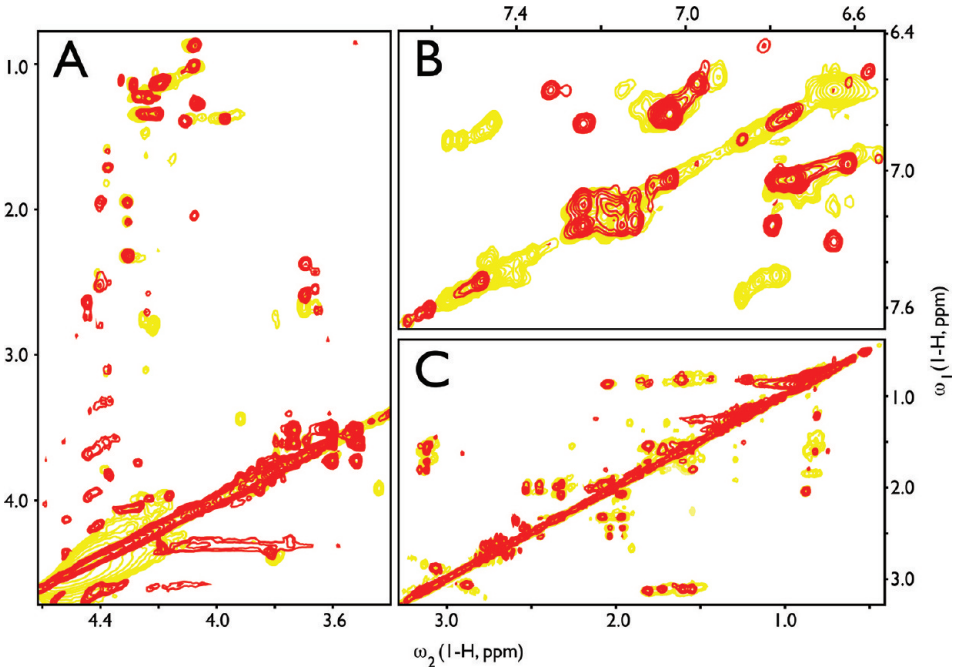

Figure 2. Overlay 900 MHz ^{1}H TOCSY spectra of 100 μM apo-AP7 in a 90% (v/v) UDDW/10% (v/v) D_2O mixture at 298 K and pH 4.0 (oligomeric, yellow) and pH 10 (monomeric, red): (A) backbone H_α, side chain methyl, side chain methylene fingerprint region, (B) side chain aryl, amide, guanidinium fingerprint region, and (C) side chain methylene fingerprint region. ^{1}H NMR chemical shifts are referenced from internal d_4-TSP.

Electrostatic Surface and Solvent Accessible Area Calculations for AP7N and AP7C. To gain further insight into electrostatic-based self-assembly of AP7N and AP7C, we utilized the NMR-determined lowest-energy structures of AP7N[17] and AP7C[15] fragments to determine the corresponding Poisson–Boltzmann solvation energies (vacuum to solvent transfer) and molecular surface plots at pH 8.0 using the PDB2PQR charge assignment (CHARMM19)[26] and Adaptive Poisson–Boltzmann Solver (APBS) solvation calculation module[27] within Python Molecular Viewer version 1.5.4 (MGL Tools, Scripps Research Institute, La Jolla, CA). For both sequences, the solvation parameters utilized a linearized Poisson–Boltzmann method, single Debye–Huckel boundary conditions, a spline-based surface smoothing method, a protein dielectric of 2.0, a solvent dielectric of 78.54, a solvent probe radius of 1.4 Å, and a system temperature of 298 K.

RESULTS

The Oligomerization of AP7 Is pH-Dependent. Previously, we observed the formation of aragonite-containing AP7 supramolecular assemblies within in vitro mineralization assays under nonreducing conditions.[11] The starting solution for these assays had a pH of approximately 3–4, and after the introduction of $(NH_4)_2CO_3$ vapor, the final assay pH was approximately 8.1–8.3 after 16 h.[5,8,11,19,20] Hence, an alkaline pH shift occurs during the nucleation and supramolecular assembly processes, and thus, like that of other nacre sequences,[22] the formation of AP7 complexes may be pH-dependent.

To assess this, we investigated the oligomerization of the apo-AP7 protein (100 μM) over a pH range of 4–11 in buffered solutions under nonreducing conditions using DLS (Figure 1). Note that we utilize the R_H values to determine the relative differences in particle sizes under different buffer conditions. We will first discuss the events that occur within the pH range of 4–9. Here, we found that the AP7 protein exists in an oligomeric state with polydispersity values of >15%, indicating that the AP7 particles are heterodisperse.[9,18,25] At pH 4, the hydrodynamic radius, R_H, of AP7 is 100.8 ± 16.3 nm, and this value was found to be concentration-independent over the range of this study [i.e., 25–100 μM (data not shown)]. In the pH range of 4.5–9.0, the R_H scattering intensity exceeds the maximum detection limit of the instrument. This is schematically portrayed on corresponding histogram bars as an arrow pointing toward higher R_H values, reflecting a dramatic increase in either the number or the average size of the protein particles in solution.[9,18,25] We note that other nacre protein sequences have also exhibited out-of-range particle sizes or numbers under identical conditions.[18] The high scattering index at pH ≥5 represents a further increase in the level of AP7 oligomerization[25] and correlates with the appearance of micrometer-sized supramolecular assemblies in mineralization assays.[11]

At pH >9, we note a dramatic decrease in AP7 particle size (R_H = 20.8 ± 10.1 nm at pH 9.5; R_H = 1.2 ± 0.3 nm at pH 10) (Figure 1), which indicates that AP7 oligomers are unstable within this pH range. The R_H value of 1.2 ± 0.3 nm corresponds to a molecular mass of approximately 7 kDa, and thus at pH 10, the monomeric form of AP7 is preferred. We confirmed these findings by conducting ^{1}H NMR TOCSY experiments with 100 μM AP7 at pH 4.0 (oligomeric) and pH 10 (monomeric) (Figure 2) and searching for evidence of oligomer-related cross-peak intensity and frequency changes. Overlay TOCSY spectra reveal that there are pH-dependent spectral differences. First, we note differences in ^{1}H chemical shifts for backbone CH_α and side chain methyl, methylene, and aryl ring protons, indicating that conformational differences exist between oligomeric and monomeric AP7 molecules.[9,28–30] Second, we note that there are TOCSY cross-peaks present in the pH 10 spectra that are absent from the pH 4 spectra. From previous NMR studies,[28–30] we know that protein oligomeriza-

dx.doi.org/10.1021/bi201346d | Biochemistry 2011, 50, 8880–8887

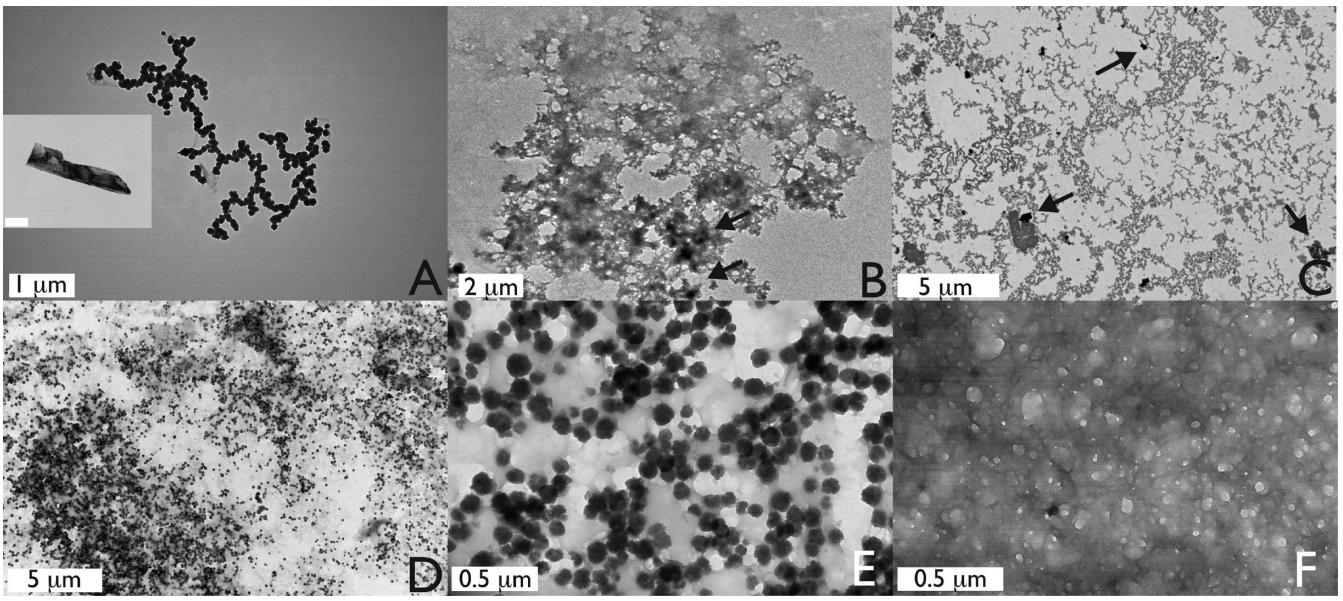

Figure 3. Transmission electron micrographs of deposits recovered from assay supernatants: (A) negative control (no peptide) [note that typical deposits are either chainlike or single-crystal forms (inset image, scale bar of 0.5 μm)], (B) 100 μM AP7 [note electron-dense deposits within the protein matrix (arrows)], (C) 100 μM AP7N [deposits appear chainlike or clustered and contain electron-dense material (arrows)], and (D–F) 100 μM C-RING AP7C. The number of deposits appears greater than the number observed for either control or AP7N scenarios. Images E and F represent higher-magnification images of single-crystal mineral deposits and matrixlike material, respectively, formed by AP7C in solution.

tion leads to attenuation of scalar cross-peak intensities due to the formation of intermolecular contacts and subsequent intermediate time scale broadening. Hence, at pH 4, there are more intermolecular interactions (oligomeric), and at pH 10, there are far fewer (monomeric), which correlates with our DLS data (Figure 1). In summary, we find that under nonreducing conditions, AP7 is monomeric at pH 10 and exists as a high-molecular mass oligomer from pH 4 to 9 in solution. The pH dependency of AP7 oligomerization indicates that side chain electrostatics[18,31−35] play an important role in AP7 protein−protein interactions. Note that line width broadening effects arising from large particle sizes and base-catalyzed solvent−backbone amide exchange preclude direct NMR structural studies of AP7 in either the oligomeric (pH 4) or the monomeric (pH 10) form (Figure 2) at this time.

pH-Dependent Self-Assembly of AP7 Domains. To assess the participation of AP7N and AP7C in AP7 oligomerization, we determined the individual assembly capabilities of AP7N and AP7C in solution using DLS (Figure 1). Here, we utilized the R_H values to determine the relative differences in particle sizes formed by the three polypeptides. These experiments revealed that both sequences oligomerize over the pH range of 4−9, but with striking differences. At pH 4, both AP7N (R_H = 2.3 ± 1.6 nm) and AP7C (1.8 ± 0.3 nm) are nearly identical in terms of R_H values and exist as a mixture of monomeric and oligomeric species. From pH 5 to 9, oligomerization predominates for both sequences, and it is the AP7C sequence that forms larger or more numerous protein particles, similar to those observed for AP7 (i.e., out of detection range). In contrast, the AP7N R_H scattering intensities remain within the range of detection and reach a maximum value of 79.7 ± 26.8 nm at pH 5 and plateau at 44.1 ± 20 nm from pH 6 to 9. Both AP7N and AP7C particles have polydispersity values of >15%, indicating that these particles are heterodisperse.[18,25] At pH >9, the R_H values for both peptides decrease (AP7N R_H ~ 7−9 nm; AP7C R_H ~ 2−13 nm) but do not attain monomeric values, indicating that both sequences form smaller oligomers under these conditions. In contrast, under these same conditions, the AP7 protein is primarily monomeric (Figure 1). From these results, we conclude that both AP7N and AP7C exist in an oligomeric state in the pH range of 5−9, and it is likely that both assembly processes are driven by side chain electrostatics.[18,31−35] However, compared to AP7N, the C-RING-like AP7C sequence forms larger or more numerous polypeptide particles in solution, similar to what we observe for the AP7 protein (Figure 1).

Mineralization Activity of AP7 Domains. Having established the self-assembly capabilities of AP7N and AP7C sequences (Figure 1), we now assess the nucleation capabilities of both domains using AP7-based mineralization assays and supernatant sampling techniques (Figures 3 and 4). Supernatants recovered from negative control assays contained single-crystal calcite (inset image, Figure 3A; Figure S1 and Table S1 of the Supporting Information) and chainlike arrangements of round deposits (Figure 3A). As reported elsewhere, AP7 assay supernatants contain amorphous-appearing complexes that contain electron-dense deposits (Figure 3B).[11] AP7N assay samples contained irregular chainlike and clustered assemblies that contained a limited number of electron-dense particles (Figure 3C, note arrows). In contrast, supernatants recovered from AP7C assays contain numerous electron-dense round deposits that are associated with a dense matrixlike material (Figure 3D–F), similar to what is typically recovered from AP7 assays (Figure 3B) as well as other intracrystalline nacre polypeptide assays.[20] These TEM images correlate with our DLS findings: AP7N and AP7C both self-assemble in solution, with the AP7C C-RING-like sequence forming particles that are comparable to those formed by AP7 (Figure 1).

Electron diffraction patterns obtained for single-crystal deposits nucleated by AP7N and AP7C reveal interesting differences compared to control scenarios that yielded only

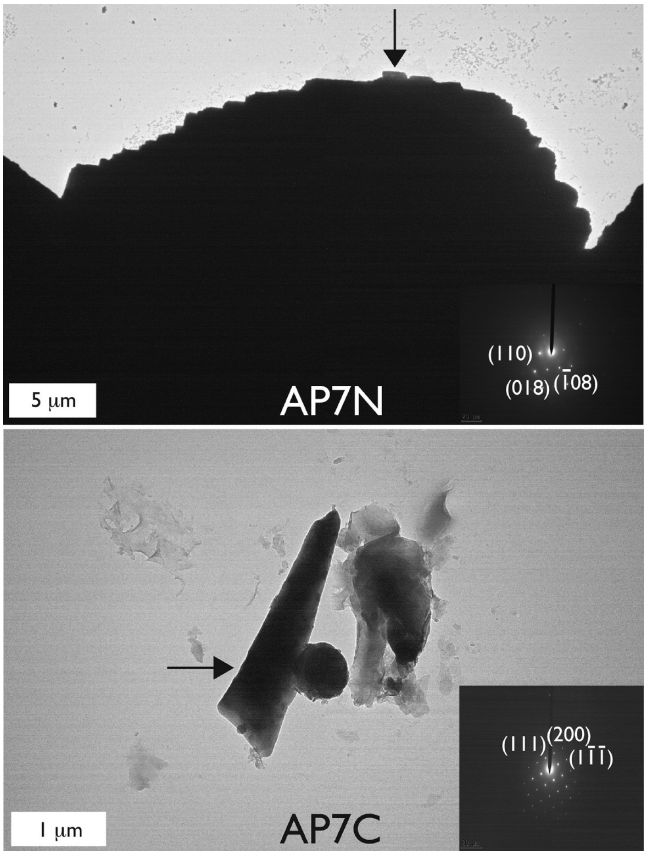

Figure 4. Transmission electron micrograph and corresponding electron diffraction pattern of typical mineral crystals recovered from 100 μM AP7N (top) and 100 μM AP7C (bottom) mineralization assay supernatants. In the top panel, the diffraction pattern taken from the protruding crystallite encircled in the main figure unambiguously matches that of calcite. The lattice parameters obtained from both diffraction patterns can be found in Table 1. For reference, geologic calcite lattice parameters (WWW-Mincryst Card 706[34]) are as follows: $a = b = 0.49896$ nm, $c = 1.7061$ nm, $\alpha = \beta = 90°$, and $\gamma = 120°$. In the bottom panel, the diffraction pattern taken from this crystal unambiguously matches that of aragonite. For reference, geologic aragonite lattice parameters (WWW-Mincryst Card 298[34]) are as follows: $a = 0.49611$ nm, $b = 0.79672$ nm, $c = 0.57404$ nm, $\alpha = \beta = \gamma = 90°$.[36]

calcite (Figure S1 of the Supporting Information). Mineral clusters produced by AP7N were found to be exclusively single-crystal calcite [10 of 10 crystals assayed (Figure 4A and Table 1)], whereas crystals produced by AP7C were found to be single-crystal calcite (9 of 10 crystals assayed) similar to that shown in Figure 4A and Table 1 and, in limited instances, single-crystal aragonite [1 of 10 crystals assayed (Figure 4B and Table 1)].[36] Obviously, the formation of single-crystal aragonite is not statistically significant in these studies, and we note that AP7C does not generate ordered lamellar or clustered single-crystal aragonite assemblies that are typical of AP7.[11] On the basis of these observations, we conclude that both AP7N and AP7C sequences nucleate single-crystal calcium carbonates in solution, with the C-RING-like AP7C sequence exhibiting a very limited ability to nucleate aragonite.

Differences in pH-Dependent Assembly Are Linked to Molecular Surface Electrostatics. The observation that AP7C forms pH-dependent particles similar to those formed by AP7 (Figure 1) suggests that there are molecular features

Table 1. Experimental d Spacing and θ Angle Values Obtained for Mineral Deposits within AP7N and AP7C Assemblies (Figure 4)[a]

deposit	lattice parameter	theoretical	experimental
AP7C aragonite	$d_{(1\,1\,1)}$	0.339 nm	0.339 nm
	$d_{(2\,0\,0)}$	0.248 nm	0.249 nm
	$d_{(1\,\bar{1}\,\bar{1})}$	0.339 nm	0.340 nm
	$\theta_{(1\,1\,1),(2\,0\,0)}$	46.8°	47°
	$\theta_{(2\,0\,0),(1\,\bar{1}\,\bar{1})}$	46.8°	47°
	$\theta_{(1\,1\,1),(1\,\bar{1}\,\bar{1})}$	93.6°	94°
AP7N calcite	$d_{(1\,1\,0)}$	0.125 nm	0.125 nm
	$d_{(0\,1\,8)}$	0.096 nm	0.095 nm
	$d_{(\bar{1}\,0\,8)}$	0.096 nm	0.095 nm
	$\theta_{(1\,1\,0),(0\,1\,8)}$	67.5°	67°
	$\theta_{(0\,1\,8),(\bar{1}\,0\,8)}$	45.1°	45°
	$\theta_{(1\,1\,0),(\bar{1}\,0\,8)}$	112.6°	112°

[a]Geologic aragonite lattice parameters were taken from WWW-Mincryst Card 298: $a = 0.49611$ nm, $b = 0.79672$ nm, $c = 0.57404$ nm, $\alpha = \beta = \gamma = 90°$. Geologic calcite lattice parameters were taken from WWW-Mincryst Card 706: $a = b = 0.49896$ nm, $c = 1.7061$ nm, $\alpha = \beta = 90°$, and $\gamma = 120°$.[36]

found within AP7C that are important for AP7 assembly. The NMR-determined structures of the AP7N[17] and AP7C[15] polypeptides are available for comparison but have yet to be jointly analyzed with regard to structural features, molecular surface electrostatics, and how these features might impact self-assembly and nucleation. Thus, we utilized the NMR-determined coordinates of the lowest-energy structures of AP7N[17] and AP7C[15] (Figure 5) and calculated the Poisson–

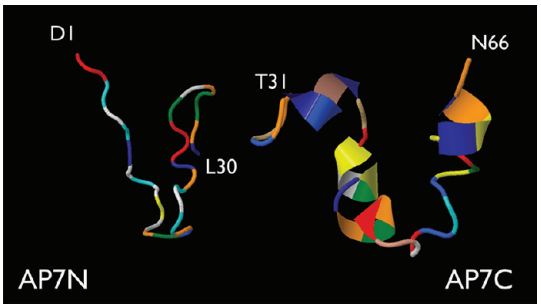

Figure 5. XPLOR-NIH-simulated annealing/molecular dynamics lowest-energy backbone structures (tube representation) of apo-AP7N and AP7C polypeptides.

Boltzmann solvent accessible molecular surfaces for both polypeptides at pH 8.0 (mineralization assay conditions) (Figure 6). The lowest-energy structure of AP7N (Figure 5) highlights the intrinsically disordered[11−14,28−30,40] conformation of this sequence (extended loop random coil structure), and this contrasts with the partially structured AP7C C-RING domain[15] that consists of three short α-helical segments and one β-turn segment, with each segment linked to another by looplike random coil intervening segments.[15] However, we observe striking differences between these sequences with regard to solvent accessible electrostatic surfaces (Figure 6). Here, both domains possess cationic and anionic electrostatic regions, with the AP7N featuring greater anionic (carboxylate, Tyr, Ser, Thr-OH, and backbone carbonyl) than cationic (R14 guanidinium) surface charge. In contrast, the AP7C sequence features significant cationic surfaces (generated by R32, H33,

dx.doi.org/10.1021/bi201346d | Biochemistry 2011, 50, 8880–8887

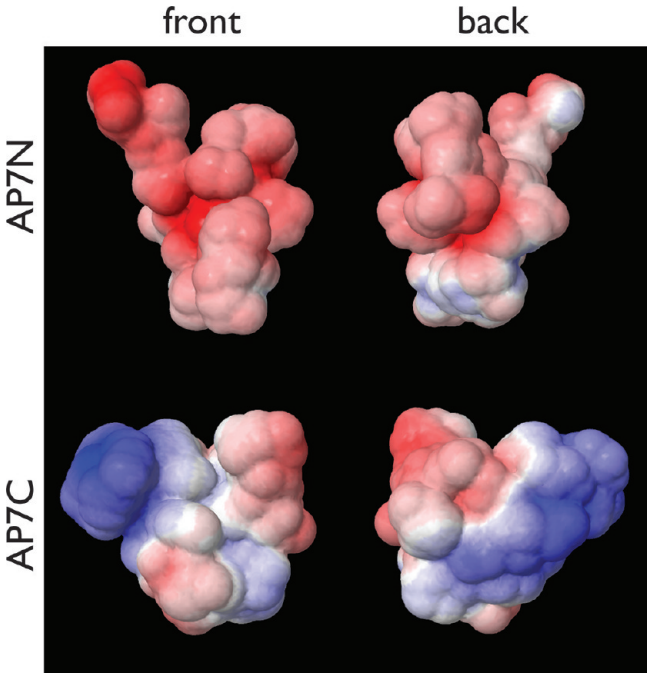

Figure 6. Calculated APBS solvent accessible electrostatic molecular surface of apo-AP7N and AP7C lowest-energy conformers (full atom representation). The "front" orientation of each molecule is consistent with the backbone orientations presented in Figure 5; the opposing side or "back" orientation of each molecule is also presented for comparison. Electrostatic surface rendering: red for anionic, blue for cationic, and white for neutral.

R36, R37, H40, R54, and R56) that complement the corresponding anionic surfaces (generated by T31, E41, Y46, S47, T49, D50, E53, D59, C42, C45, C57, T61, C62, Y64, T65, and backbone carbonyl groups) on either side of the molecule, a feature not found in AP7N. The fact that both AP7N and AP7C feature cationic−anionic surface charge regions explains why both sequences self-associate and oligomerize in a pH-dependent fashion in solution (Figure 1). However, we believe that the significant and complementary surface charge distribution found on the C-RING domain (Figure 6) explains in part why AP7C forms large particle sizes (Figure 1) and denser matrix deposits (Figure 3) compared to those of AP7N. We believe that the unique surface charge features of AP7C most likely contribute to the pH-dependent oligomeric assembly of AP7 in solution (Figures 1−3) and play a role in aragonite formation, as well (Figure 4).

■ DISCUSSION

This study reveals that an intrinsically disordered extracellular matrix protein, AP7, spontaneously oligomerizes within the pH range found in in vitro mineralization assays (pH 4−8)[11] and forms heterogeneously sized protein particles (Figure 1) that feature protein−protein intermolecular contacts (Figure 2). These new data now explain why AP7 formed supramolecular assemblies under mineralization assay conditions[11] and demonstrate that AP7 oligomerization is linked to the self-associative properties of its N- and C-terminal domains (Figures 1 and 3). However, it is the C-RING-like imitator domain (AP7C) that most closely resembles AP7 with regard to oligomerization properties (Figure 1) and morphologies (Figure 3). The observed similarities in AP7 and AP7C oligomerization are most likely linked to the significant anionic−cationic complementary surface charge distribution found on AP7C (Figure 6). This complementary distribution would allow both AP7 and AP7C to strongly self-associate in a pH-dependent fashion (Figures 1 and 3). Thus, the C-RING-like imitator sequence plays an important role in AP7 oligomerization, and these findings are consistent with the known role of RING sequences as protein−protein interactive domains within intracellular proteins.[21−24]

The oligomerization of AP7 and those of its sequence fragments are pH-dependent processes (Figure 1), and we conclude that protein−protein side chain ion pairing[34−38] is a potential driving force in AP7 supramolecular assembly. The major stage of oligomerization (pH 4−4.5) corresponds with the pK_a values for most protein Asp and Glu residue carboxylate groups.[38−40] In AP7, these anioinic residues are evenly distributed within both domains (D1, D2, D21, and D22 in AP7N and E41, D50, E53, and D59 in AP7C) (Figure 1). We hypothesize that these carboxylate groups form intermolecular salt bridges with cationic groups such as His and Arg on other AP7 molecules. We also note that the dissociation of AP7 oligomers is initiated at pH >9, which is near the pK_a range of Cys thiol groups (8.0−9.0), and from this, we conclude that Cys side chains also participate in the self-association process.[38−40] Another interesting feature with regard to cationic groups is their intramolecular distribution within the AP7 sequence. With the exception of R14 (AP7N), the bulk of the cationic groups are located within AP7C (R32, H33, R36, R37, H40, R54, and R56). This uneven distribution of cationic residues further supports the notion that C-RING AP7C is an important site for AP7−AP7 protein electrostatic interactions (Figure 6). Additional studies will be required to identify specific ion pairing participants in the oligomerization process and to identify nonbonding interactions, such as van der Waals/hydrophobic, aryl ring−ring, or hydrogen bonding interactions[9,22] that further stabilize AP7 oligomers.

Finally, our results clearly document the first known instance of a RING-like sequence assembling to form a polypeptide matrix that subsequently nucleates single-crystal calcium carbonates. This unusual finding raises some important questions about the potential function(s) of RING domains in other proteins, and we anticipate that further genomic and proteomic research will uncover other interesting variations in RING sequence and function. However, we caution the reader that our results do not imply that AP7N has no role to play in either AP7 oligomerization or mineralization. One should note that there are discrepancies between AP7 and AP7C in terms of oligomer morphology (Figure 3), oligomer dissociation at alkaline pH (Figure 1), and aragonite formation (Figures 3 and 4).[11] Moreover, solvation electrostatic calculations clearly demonstrate that AP7N possesses regions of anionic surface charge that could form ion pairs with the cationic regions found on AP7C (Figure 6) and thus promote protein−protein interactions. Thus, we stress that AP7N is an important contributor to AP7 function, and there may be cooperative interactions involving both AP7C and AP7N regions during AP7 oligomerization and nucleation. The functional role of AP7N and its interactions with AP7C will be the focus of our subsequent research.

■ ASSOCIATED CONTENT

Supporting Information

Representative transmission electron micrograph of calcium carbonate crystals recovered from control assays (no peptide

added, bovine serum albumin added) (Figure S1 and Table S1). This material is available free of charge via the Internet at http://pubs.acs.org.

AUTHOR INFORMATION

Corresponding Author

*Telephone: (212) 998-9605. Fax: (212) 995-4087. E-mail: jse1@nyu.edu.

Funding

Supported by the U.S. Department of Energy, Office of Basic Energy Sciences, Division of Materials Sciences and Engineering, via Grant DE-FG02-03ER46099.

ACKNOWLEDGMENTS

This is contribution 60 from the Laboratory for Chemical Physics, New York University.

ABBREVIATIONS

AP7, aragonite protein 7 from *Haliotis rufescens*; AP7C, 36-amino acid C-terminal domain of the AP7 protein; AP7N, 30-amino acid N-terminal domain of the AP7 protein; IDP, intrinsically disordered protein; UDDW, unbuffered deionized distilled water; DLS, dynamic light scattering; RING, really interesting new gene; C-RING, RING domain, C subclass; ACC, amorphous calcium carbonate.

REFERENCES

(1) Shen, X., Belcher, A. M., Hansma, P. K., Stucky, G. D., and Morse, D. E. (1997) Molecular cloning and characterization of Lustrin A, a matrix protein from shell and pearl nacre of *Haliotis rufescens*. *J. Biol. Chem. 272*, 32472−32481.

(2) Samata, T., Hayashi, N., Kono, M., Hasegawa, K., Horita, C., and Akera, S. (1999) A new matrix protein family related to the nacreous layer formation of *Pinctada fucata*. *FEBS Lett. 462*, 225−232.

(3) Ma, Z., Huang, J., Sun, J., Wang, G., Li, C., Xi, L., and Zhang, R. (2007) A novel extrapallial fluid protein controls the morphology of nacre lamellae in the pearl oyster, *Pinctada fucata*. *J. Biol. Chem. 282*, 23253−23260.

(4) Suzuki, M., Saruwatari, K., Kogure, T., Yamamoto, Y., Nishimura, T., Kato, T., and Nagasawa, H. (2009) An acidic matrix protein, Pif, is a key macromolecule for nacre formation. *Science 325*, 1388−1390.

(5) Michenfelder, M., Fu, G., Lawrence, C., Weaver, J. C., Wustman, B. A., Taranto, L., and Evans, J. S. (2003) Characterization of two molluscan crystal-modulating biomineralization proteins and identification of putative mineral binding domains. *Biopolymers 70*, 522−533. (2004) *73*, 291 (erratum).

(6) Fu, G., Qiu, S. R., Orme, C. A., Morse, D. E., and DeYoreo, J. J. (2007) Acceleration of calcite kinetics by nacre proteins. *Adv. Mater. 17*, 2678−2683.

(7) Falini, G., Albeck, S., Weiner, S., and Addadi, L. (1996) Control of aragonite or calcite polymorphism by mollusk shell macromolecules. *Science 271*, 67−69.

(8) Ndao, M., Keene, E., Amos, F. A., Rewari, G., Ponce, C. B., Estroff, L., and Evans, J. S. (2010) Intrinsically disordered mollusk shell prismatic protein that modulates calcium carbonate crystal growth. *Biomacromolecules 11*, 2539−2544.

(9) Delak, K., Harcup, C., Lakshminarayanan, R., Zhi, S., Fan, Y., Moradian-Oldak, J., and Evans, J. S. (2009) The tooth enamel protein, porcine amelogenin, is an intrinsically disordered protein with an extended molecular configuration in the monomeric form. *Biochemistry 48*, 2272−2281.

(10) Mann, K., Siedler, F., Treccani, L., Heinemann, F., and Fritz, M. (2007) Perlinhibin, a cysteine, histidine, and arginine-rich miniprotein from abalone (*Haliotis laevigata*) nacre, inhibits in vitro calcium carbonate crystallization. *Biophys. J. 93*, 1246−1252.

(11) Amos, F. F., and Evans, J. S. (2009) AP7, a partially disordered pseudo C-RING protein, is capable of forming stabilized aragonite in vitro. *Biochemistry 48*, 1332−1339.

(12) Uversky, V. N. (2002) Natively unfolded proteins: A point where biology waits for physics. *Protein Sci. 11*, 739−756.

(13) Uversky, V. N., Gillespie, J. R., and Fink, A. L. (2000) Why are "natively unfolded" proteins unstructured under physiologic conditions? *Proteins 41*, 415−427.

(14) Meng, J., Romero, P., Yang, J. Y., Chen, J. W., Vacic, V., Obradovic, Z., and Uversky, V. N. (2008) The unfoldomics decade: An update on intrinsically disordered proteins. *BMC Genomics 9*, 1−26.

(15) Collino, S., Kim, I. W., and Evans, J. S. (2008) Identification and structural characterization of an unusual RING-like sequence within an extracellular biomineralization protein, AP7. *Biochemistry 47*, 3745−3755.

(16) Kim, I. W., Collino, S., Morse, D. E., and Evans, J. S. (2006) A crystal modulating protein from molluscan nacre that limits the growth of calcite *in vitro*. *Cryst. Growth Des. 6*, 1078−1082.

(17) Collino, S., and Evans, J. S. (2007) Structural features that distinguish kinetically distinct biomineralization polypeptides. *Biomacromolecules 7*, 1686−1694.

(18) Amos, F. F., Ponce, C. B., and Evans, J. S. (2011) Formation of framework nacre polypeptide supramolecular assemblies that nucleate polymorphs. *Biomacromolecules 12*, 1883−1889.

(19) Keene, E. C., Evans, J. S., and Estroff, L. A. (2010) Silk fibroin hydrogels coupled with the n16N-β-chitin complex: An in vitro organic matrix for controlling calcium carbonate mineralization. *Cryst. Growth Des. 10*, 5169−5175.

(20) Amos, F. F., Destine, E., Ponce, C. B., and Evans, J. S. (2010) The N- and C-terminal regions of the pearl-associated EF hand protein, PFMG1, promote the formation of the aragonite polymorph in vitro. *Cryst. Growth Des. 10*, 4211−4216.

(21) Saurin, A. J., Borden, K. L. B., Boddy, M. N., and Freemont, P. S. (1996) Does this have a familiar RING? *Trends Biochem. Sci. 21*, 208−215.

(22) Freemont, P. S. (2000) Ubiquitination: RING for destruction? *Curr. Biol. 10*, R84−R87.

(23) Capili, A. D., Edghill, E. L., Wu, K., and Borden, K. L. B. (2004) Structure of the C-terminal RING finger from a RING-IBR-RING/TRIAD motif reveals a novel zinc-binding domain distinct from a RING. *J. Mol. Biol. 340*, 1117−1129.

(24) Borden, K. L. B. (2000) RING domains: Master builders of molecular scaffolds? *J. Mol. Biol. 295*, 1103−1112.

(25) Schärtl, W. (2007) *Light scattering from polymer solutions and nanoparticle dispersions*, 1st ed., Springer-Verlag, Heidelberg, Germany.

(26) Dolinsky, T. J., Nielsen, J. E., McCammon, J. A., and Baker, N. A. (2004) PDB2PQR: An automated pipeline for the setup, execution, and analysis of Poisson-Boltzmann electrostatics calculations. *Nucleic Acids Res. 32*, 665−667.

(27) Baker, N. H., Sept, D., Joseph, S., Holst, N. J., and McCammon, J. A. (2001) Electrostatics of nanosystems: Application to microtubules and the ribosome. *Proc. Natl. Acad. Sci. U.S.A. 98*, 10037−10041.

(28) Ndao, M., Dutta, K., Bromley, K., Sun, Z., Lakshminarayanan, R., Rewari, G., Moradian-Oldak, J., and Evans, J. S. (2011) Probing the self-association, intermolecular contacts, and folding propensity of amelogenin. *Protein Sci. 20*, 724−734.

(29) Buchko, G. W., Tarasevich, B. J., Bekhazi, J., Snead, M. L., and Shaw, W. J. (2008) A solution NMR investigation into the early events of amelogenin nanosphere self-assembly. *Biochemistry 47*, 13215−13222.

(30) Li, M., Liu, J., Ran, X., Fang, M., Shi, J., Qin, H., Goh, J. M., and Song, J. (2006) Resurrecting abandoned proteins with pure water: CD and NMR studies of protein fragments solubilized in salt-free water. *Biophys. J. 91*, 4201−4209.

(31) Shera, J. N., and Sun, X. S. (2009) Effect of peptide sequence on surface properties and self-assembly of an amphipathic pH-responsive peptide. *Biomacromolecules 10*, 2446−2450.

(32) Zimenkov, Y., Dublin, S. N., Ni, R., Tu, R. S., Breedveld, V., Apkarian, R. P., and Conticello, V. P. (2006) Rational design of a reversible pH-responsive switch for peptide self-assembly. *J. Am. Chem. Soc. 126*, 6770−6771.
(33) Dalmau, M., Lim, S., and Wang, S. W. (2009) pH-triggered disassembly in a caged protein complex. *Biomacromolecules 10*, 3199−3206.
(34) Kayser, V., Turton, D. A., Aggeli, A., Beevers, A., Reid, G. D., and Beddard, G. S. (2004) Energy migration in novel pH-triggered self-assembled β-sheet ribbons. *J. Am. Chem. Soc. 126*, 336−343.
(35) Rajagopal, K., Lamm, M. S., Haines-Butterick, L. A., Pochan, D. J., and Schneider, J. P. (2009) Tuning the pH responsiveness of β-hairpin peptide folding, self-assembly, and hydrogel material formation. *Biomacromolecules 10*, 2619−2625.
(36) Chichagov, A. V., Varlamov, D. A., Dilanyan, R. A., Dokina, T. N., Drozhzhina, N. A., Samokhvalova, O. L., and Ushakovskaya, T. V. (2001) MINCRYST: A crystallographic database for minerals, local and network (WWW) versions. *Crystallogr. Rep. 46*, 876−879.
(37) Ndao, M., Keene, E., Amos, F. A., Rewari, G., Ponce, C. B., Estroff, L., and Evans, J. S. (2010) Intrinsically disordered mollusk shell prismatic protein that modulates calcium carbonate crystal growth. *Biomacromolecules 11*, 2539−2544.
(38) Song, Y., Mao, J., and Gunner, M. R. (2009) MCCE2: Improving protein pKa calculations with extensive side chain rotamer sampling. *J. Comput. Chem. 30*, 2231−2247.
(39) Merz, K. M. (1991) Determination of pKas of ionizable groups in proteins: The pKa of Glu 7 and 35 in hen egg white lysozyme and Glu 106 in human carbonic anhydrase. *J. Am. Chem. Soc. 113*, 3572−3575.
(40) Li, H., Robertson, A. D., and Jensen, J. H. (2005) Very fast empirical prediction and rationalization of protein pKa values. *Proteins: Struct., Funct., Bioinf. 61*, 704−721.